Independence of the spin current from the Néel vector orientation in antiferromagnet CoO

M. Yang,[1,*] Q. Li,[1,*,†] D. Hou,[2] P. Shafer,[3] A. T. N'Diaye,[3] C. Klewe,[3] T. Y. Wang,[1] Xixiang Zhang,[4] C. Hwang,[5] and Z. Q. Qiu[1,‡]

[1]*Department of Physics, University of California at Berkeley, Berkeley, California 94720, USA*

[2]*International Centre for Quantum Design of Functional Materials (ICQD), Hefei National Laboratory for Physical Sciences at the Microscale (HFNL), and Synergetic Innovation Center of Quantum Information and Quantum Physics, University of Science and Technology of China, Hefei 230026, China*

[3]*Advanced Light Source, Lawrence Berkeley National Laboratory, Berkeley, California 94720, USA*

[4]*Physical Science and Engineering Division (PSE), King Abdullah University of Science and Technology (KAUST), Thuwal 23955-6900, Saudi Arabia*

[5]*Korea Research Institute of Standards and Science, Yuseong, Daejeon 305-340, Korea*

(Received 30 March 2020; accepted 29 May 2020; published 11 June 2020)

Spin pumping from ferromagnetic Fe into antiferromagnetic CoO across a Ag spacer layer was studied using ferromagnetic resonance (FMR) in Py/CoO/Ag/Fe/Ag(001). The thin Py film on top of CoO permits an alignment of the CoO Néel vector through field cooling in two otherwise equivalent [110] and [1$\bar{1}$0] crystalline axes which are parallel and perpendicular to the Fe magnetization direction, respectively. Fe FMR linewidth is measured as a function of Ag thickness in 10–20-GHz frequency range and in 180–330 K temperature range. We find that there exists an anisotropy in the Fe FMR damping for parallel and perpendicular alignment of the Fe and CoO spins. However, such anisotropic damping exists only at thin Ag thickness where there exists a magnetic interlayer coupling between Fe and CoO, and vanishes at thick Ag thickness where the interlayer coupling becomes negligible but permitting spin-current transmission into CoO. Our result indicates the absence of anisotropic spin current for parallel and perpendicular alignment of the Fe and CoO spin axes.

DOI: 10.1103/PhysRevB.101.224418

I. INTRODUCTION

Research on spin current across antiferromagnetic (AFM) insulators has attracted much interest after the demonstration of AFM NiO and CoO as excellent spin-current mediators [1–4]. It is generally believed that thermally excited AFM spin modes (magnons) are responsible for the spin-current transmission in an AFM insulator [5–8], especially in the vicinity of the Néel temperature (T_N) associated with AFM order. An important consequence of the above mechanism is that only the component of spin that is parallel to the AFM Néel vector should be transmitted. This is because AFM magnons oscillate at high frequency (THz range) compared to typical current pulses (DC to GHz) and their time-averaged spin is effectively parallel to the Néel vector [9–11]. In other words, pumping spin into an AFM should exhibit a strong anisotropic dependence on the AFM spin orientation.

It is obvious that whether or not there exists a spin current anisotropy is crucial to the understanding of spin current in AFM. Experimental verification of this anisotropic behavior of the spin current in AFM, however, seems to show inconclusive results with some reports supporting anisotropic behavior [12–17] and others that are contradictory [18–20]. The complexity in identifying the spin-current anisotropy can be traced to two critical experimental issues. First, many studies—especially those which employed polycrystalline AFM—have assumed a parallel alignment between the ferromagnetic (FM) magnetization and the AFM Néel vector. This assumption is generally not supported by experimental evidence. In fact, many FM/AFM systems are shown to have perpendicular alignment between the FM magnetization and the AFM Néel vector [21–23]. Second, there often exist other effects which coexist with the spin-current effect in the experimental measurement. For example, it was shown that measurements of the inverse spin Hall effect are also susceptible to detecting the proximity effect [24], and the interface morphology could play a role in spin Hall magnetoresistance [25], so that it is sometimes difficult to identify the spin-current contribution quantitatively. The anisotropic linewidth broadening of ferromagnetic resonance (FMR), which is usually used in spin-pumping measurements, could also arise in the FM layer from anisotropic spin relaxation, such as two-magnon scattering [26–29], and anisotropic Gilbert damping [30,31], etc. In order to prove/disprove the spin-current anisotropic effect unambiguously, which is crucial to the understanding of spin current in AFM, it is important to have a well-defined system in which the AFM Néel vector orientation can be determined directly by experiment, and to carefully account for other experimental contributions to rule out any other artifacts in the spin-current measurement.

II. EXPERIMENTAL

In this paper, we report our investigation of spin current pumped into AFM CoO from Fe (driven into FMR) across

*These authors contributed equally to this work.
†qianli2015@berkeley.edu
‡qiu@berkeley.edu

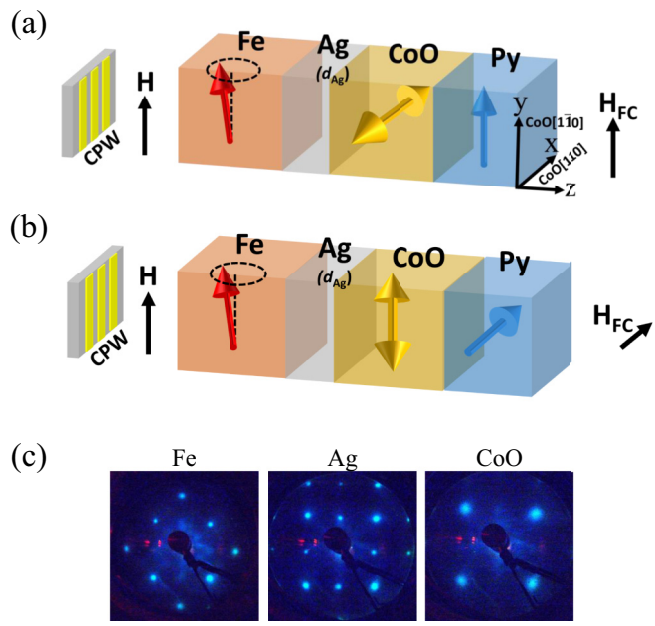

FIG. 1. (a), (b) Schematic drawing of the sample structure and FMR measurement. Here x- and y axes are defined as CoO [110] and [1$\bar{1}$0] axes, and z axis is the sample normal direction. In the FMR measurement, the external field (H) is applied along the CPW strip line direction (y axis). Thus field cooling (H_{FC}) and Py/CoO coupling create (a) perpendicular and (b) parallel alignment between the frozen CoO spin Néel vector (yellow arrows) and the Fe magnetization (red arrows). Blue arrows indicate the Py magnetization during field cooling. (c) LEED patterns from sample of MgO(3 nm)/Py(2 nm)/CoO(10 nm)/Ag(8 nm)/Fe(4 nm)/Ag(001).

a Ag spacer in a layered structure of MgO(3 nm)/Py(2 nm)/CoO(10 nm)/Ag(d_{Ag})/Fe(4 nm)/Ag(001) [Figs. 1(a) and 1(b)], where Py indicates $Ni_{80}Fe_{20}$ (permalloy). FMR has been a powerful mechanism for the study of spin pumping because the FM layer at FMR is a high-quality source of spin current that simultaneously serves as a spin-pumping indicator due to FMR linewidth broadening or damping enhancement [12,16,20,32–36]. In order to avoid experimental artifacts mentioned previously, we designed our sample by considering the following factors. First, the CoO AFM spin axis ($\overleftrightarrow{S}_{CoO}$) was controlled by the direction of an applied field (H_{FC}) when cooling below T_N with the aid of Py/CoO interfacial coupling. In this way $\overleftrightarrow{S}_{CoO}$ was deterministically aligned along one of two equivalent CoO easy axes (EA) in the film plane, [110] or [1$\bar{1}$0], "frozen" against subsequent field perturbation [22,37]. Consequently, perpendicular and parallel alignments between the Fe magnetization ($\vec{M}_{Fe}$) and the CoO Néel vector orientation were realized, with the Fe magnetization aligned to the y axis by FMR field (H) during FMR measurement [Figs. 1(a) and 1(b)]. Since both Fe and CoO spins in these two situations are always along equivalent crystal axes within each layer, any crystalline anisotropic spin relaxation effect can be ruled out in our experiment. Second, we measured the CoO Néel vector orientation directly by x-ray magnetic linear dichroism (XMLD) spectroscopy to avoid any ambiguity on the relative orientation between the Fe magnetization and the CoO Néel vector. Finally, the CoO/Ag/Fe interlayer coupling is tuned by the Ag spacer layer thickness to facilitate identification of the interlayer coupling and spin-current contributions to FMR linewidth broadening measurements. Noting that the Ag thickness range ($d_{Ag} \leqslant 8$ nm) in our experiment is well below the spin-current diffusion length in Ag (~170 nm) [38], we proceeded to carefully search for the spin-current anisotropy effect by comparing the Fe FMR linewidths for parallel ($\vec{M}_{Fe} \parallel \overleftrightarrow{S}_{CoO}$) and perpendicular ($\vec{M}_{Fe} \perp \overleftrightarrow{S}_{CoO}$) alignments between $\vec{M}_{Fe}$ and $\overleftrightarrow{S}_{CoO}$.

MgO/Py/CoO/Ag(d_{Ag})/Fe/Ag(001) multilayer samples were prepared in an ultrahigh vacuum system by molecular-beam epitaxy (MBE). The Ag(001) substrates were prepared by cycles of Ar^+ ion sputtering at 2 keV and annealing at 500 °C. A 4-nm Fe film was deposited onto the Ag(001) substrate. Then, a Ag film was deposited with thickness of 2, 2.5, 3, 4.5, 6, and 8 nm for six samples, respectively. A 10-nm-CoO film was grown by evaporating Co at an oxygen atmosphere of 2.0×10^{-6} Torr. Then half of the sample surface was coated by a 2-nm Py film. Finally, a 3-nm MgO capping layer was deposited on the entire sample for protection of the metallic layers against ambient oxidation. All films were grown at room temperature. In the sample structure, the Fe, Ag, and CoO layers are epitaxially grown with the in-plane lattice relation of CoO[110] ∥ Ag[110] ∥ Fe[100] ∥ Ag[110] [see the low-energy electron diffraction (LEED) patterns in Fig. 1(c)]. FMR measurements were performed by placing the sample on top of a coplanar waveguide (CPW) in the temperature range of 180 to 320 K. FMR signal was detected by collecting the field derivative of the absorption intensity. FMR signal of 4-nm Fe layer and 2-nm Py layer can be distinguished by different resonance field [39] and resonance intensity [40]. In fact, the Py FMR signal below the CoO Néel temperature is virtually invisible in our system. Hysteresis loops of the Fe and Py layers were obtained by magneto-optical Kerr effect (MOKE) measurements on the half of sample without Py layer and x-ray magnetic circular dichroism (XMCD) spectroscopy with x-ray photon energy tuned at Ni absorption peak, respectively. XMCD and XMLD measurements were performed at beamlines 4.0.2 and 6.3.1 of the Advanced Light Source.

III. RESULTS AND DISCUSSIONS

We first studied the interlayer coupling between Fe and CoO across the Ag spacer layer in CoO/Ag/Fe/Ag(001) by measuring the Fe hysteresis loops after field cooling [Figs. 2(a) and 2(b)]. Square easy-axis hysteresis loops were obtained for $H \parallel H_{FC}$ and double-split hard-axis (HA) loops were obtained for $H \perp H_{FC}$, indicating that the Fe/CoO interlayer coupling has induced an in-plane uniaxial anisotropy in the Fe film with the EA parallel to H_{FC} which is consistent with literature results [41]. Both the coercivity (H_C) and the shifted field (H_S, defined in Fig. 2(b), which is proportional to the uniaxial anisotropy [42]) decrease with increasing Ag thickness and approach constant values for d_{Ag} above 4.5 nm [43] [see the summary result shown later in Fig. 3(e)]. It should be mentioned that the interlayer coupling between Fe and CoO layers across a thin Ag layer could even exhibit weak oscillatory behavior for very high-quality films [43], but the

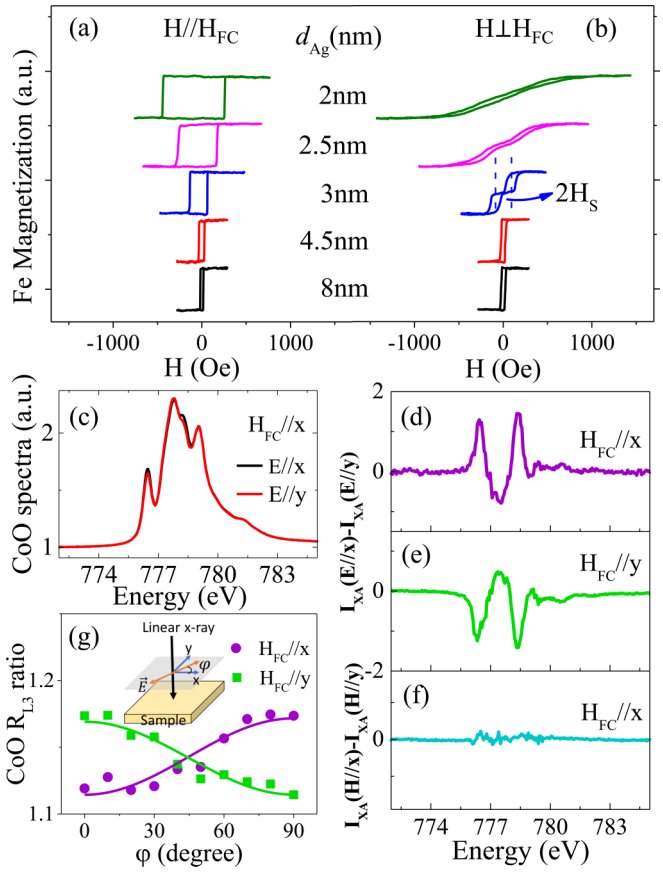

FIG. 2. Fe hysteresis loops for (a) $H \parallel H_{FC}$ and (b) $H \perp H_{FC}$. The interlayer coupling between Fe and CoO decreases with increasing Ag thickness and vanishes above 4.5-nm Ag thickness. (c) CoO spectra measured with linear polarized x rays for $H_{FC} \parallel x$. XMLD spectra of (d) $H_{FC} \parallel x$ and (e) $H_{FC} \parallel y$ are equal and opposite, confirming that CoO spins are aligned along y and x directions, respectively. (f) The unchanged XMLD (with fixed x-ray polarization, $E \parallel x$ and $E \parallel y$) after rotating a 4000-Oe field from x to y axis proves the frozen CoO spins after field cooling. (g) The CoO R_{L3} ratio exhibits $\cos^2\varphi$ dependence on x-ray polarization angle (φ), showing that CoO spins are aligned perpendicularly to H_{FC}. Solid lines are cosine fits to the data. Inset shows the schematic of XMLD measurement, with φ defined as the angle between x-ray polarization and x axis. All measurements were performed at 200 K.

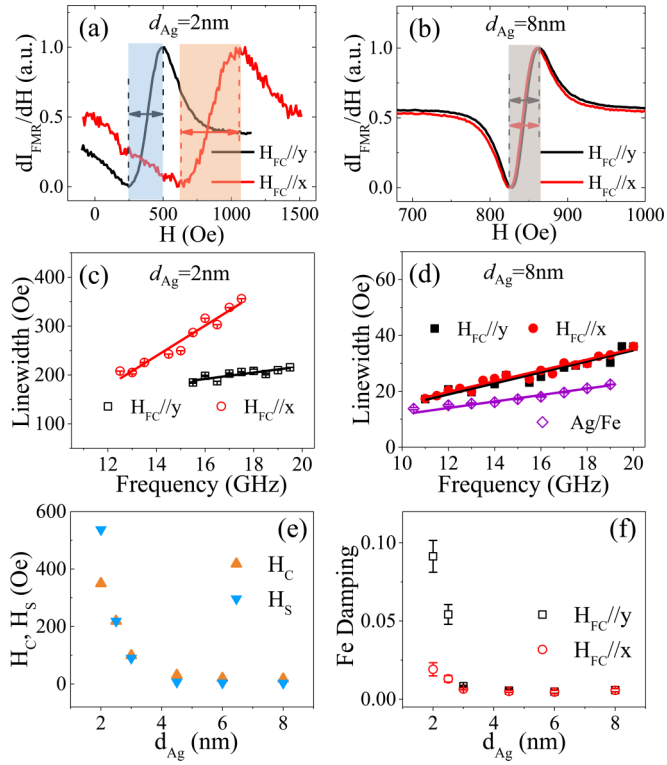

FIG. 3. Fe FMR spectra measured at 17.5 GHz with $H_{FC} \parallel x$ and $H_{FC} \parallel y$ in (a) $d_{Ag} = 2$-nm sample and (b) $d_{Ag} = 8$-nm sample. The shading with arrows indicates the FMR full linewidth ($2\Delta H$). Frequency-dependent FMR linewidth (ΔH) for $H_{FC} \parallel y$ and $H_{FC} \parallel x$ from (c) $d_{Ag} = 2$-nm sample and (d) $d_{Ag} = 8$-nm sample. Solid lines are fitting with Eq. (1). The linewidth from a reference sample of Ag(8 nm)/Fe(4 nm) is also shown in (d) to indicate the existence of spin-current pumping into CoO. (e) Coercivity (H_C), splitting field (H_S), and (f) FMR damping of Fe layer as a function of the Ag spacer layer thickness. All measurements were performed at 200 K.

coupling usually decreases monotonically with spacer layer thickness when films become rougher than epitaxial metallic thin films (e.g., CoO film grown by MBE). Nevertheless the Fe/CoO interlayer coupling vanishes above 4.5-nm Ag thickness, which is important for the FMR linewidth study presented later.

We then performed XMLD spectroscopy at Co L_3 edge to determine the CoO AFM spin orientation in MgO/Py/CoO/Ag/Fe/Ag(001). Because FMR is performed by applying the magnetic field along the CPW stripe line direction [$H \parallel y$ in both Figs. 1(a) and 1(b)], we controlled the CoO spin orientation by field cooling while leveraging Py/CoO coupling under the conditions of $H_{FC} \parallel y$ [Fig. 1(a)] and $H_{FC} \parallel x$ [Fig. 1(b)], respectively. The CoO spectra measured with two orthogonal x-ray polarizations [44] [Fig. 2(c)] were used to obtain x-ray linear dichroism [Figs. 2(d) and 2(e)] for two field-cooling directions. The inverse intensity of these dichroism spectra and their comparison to previous studies [22,44] indicate that the CoO spin axis is along the y axis ($\overleftrightarrow{S}_{CoO} \parallel y$) for $H_{FC} \parallel x$ and along the x axis ($\overleftrightarrow{S}_{CoO} \parallel x$) for $H_{FC} \parallel y$, proving that the Py/CoO coupling leads to a perpendicular alignment between the Py magnetization and the CoO spin axis ($\vec{M}_{Py} \perp \overleftrightarrow{S}_{CoO}$), which is a feature of spin-flop coupling. This conclusion is further confirmed by the observed $\cos^2\varphi$ (here φ is the x-ray polarization angle) dependence of the CoO R_{L3} ratio [Fig. 2(g)], which is defined as intensity ratio of the peak at 777.8 eV over the peak at 778.2 eV. Then for the case of $H_{FC} \parallel y$ [Fig. 1(a)], the Fe FMR is under the condition of $\vec{M}_{Fe} \perp \overleftrightarrow{S}_{CoO}$. For the case of $H_{FC} \parallel x$ [Fig 1(b)], it is important to additionally verify that the CoO spins stay frozen along the y axis after the external FMR field rotates the Fe and Py magnetization from x- to y axis. Figure 2(f) shows that the CoO XMLD signal remains unchanged after switching the Fe magnetization from x- to y axis by a 4000-Oe magnetic field, proving that CoO spins remain frozen [22] along the y axis after field cooling ($H_{FC} \parallel x$). Thus for the case of $H_{FC} \parallel x$ [Fig. 1(b)], we ensure that the Fe FMR is performed under the condition of $\vec{M}_{Fe} \parallel \overleftrightarrow{S}_{CoO}$.

Next we performed Fe FMR measurements at 200 K by applying an external magnetic field (H) along the CPW strip line direction (y axis) to investigate spin pumping from the Fe layer for the two situations of $\vec{M}_{\rm Fe} \perp \overleftrightarrow{S}_{\rm CoO}$ [Fig. 1(a)] and $\vec{M}_{\rm Fe} \parallel \overleftrightarrow{S}_{\rm CoO}$ [Fig. 1(b)], respectively. We find that the Fe FMR in the $d_{\rm Ag} = 2$-nm sample produces substantially different spectra of the FMR differential intensity ($dI_{\rm FMR}/dH$) for $\vec{M}_{\rm Fe} \perp \overleftrightarrow{S}_{\rm CoO}$ and $\vec{M}_{\rm Fe} \parallel \overleftrightarrow{S}_{\rm CoO}$ [Fig. 3(a)]. First, the FMR resonance field is clearly shifted to a higher field for $\vec{M}_{\rm Fe} \parallel \overleftrightarrow{S}_{\rm CoO}$ than for $\vec{M}_{\rm Fe} \perp \overleftrightarrow{S}_{\rm CoO}$, which is consistent with the induced uniaxial anisotropy by the Fe/CoO perpendicular interlayer coupling across the Ag spacer layer [Fig. 2(b)]. Second, the FMR linewidth $2\Delta H$ (ΔH is defined as half width at half maximum from the Lorentz derivative fit) shows an obvious broadening for $\vec{M}_{\rm Fe} \parallel \overleftrightarrow{S}_{\rm CoO}$ compared to $\vec{M}_{\rm Fe} \perp \overleftrightarrow{S}_{\rm CoO}$. Since FMR linewidth at a single frequency does not necessarily reflect the intrinsic damping, we performed FMR in the frequency range of 10–20 GHz [Fig. 3(c)] to obtain the frequency-dependent FMR linewidth ΔH. It is observed that ΔH follows the expected linear dependence on frequency (f) with the slope α representing the intrinsic FMR damping [45].

$$\Delta H = \Delta H_0 + \frac{2\pi}{\mu_0 \gamma} \alpha f. \tag{1}$$

Here ΔH_0 is intercept of linewidth at zero frequency, and γ is gyromagnetic ratio with $\gamma/2\pi \approx 29.4$ GHz/T. A linear fitting (solid lines) of Fig. 3(c) using Eq. (1) yields $\alpha = 0.091$ for the case of $\vec{M}_{\rm Fe} \parallel \overleftrightarrow{S}_{\rm CoO}$ and $\alpha = 0.019$ for the case of $\vec{M}_{\rm Fe} \perp \overleftrightarrow{S}_{\rm CoO}$. Noting that there could exist different FMR damping for $H \parallel y$ and $H \parallel -y$ due to exchange bias for the case of $H_{\rm FC} \parallel y$, we also measured the FMR linewidth for $H \parallel -y$ and find the same intrinsic damping as that for $H \parallel y$. Recalling that the CoO spins are along equivalent crystal axes for the two cases of $\vec{M}_{\rm Fe} \parallel \overleftrightarrow{S}_{\rm CoO}$ and $\vec{M}_{\rm Fe} \perp \overleftrightarrow{S}_{\rm CoO}$, we conclude that the different damping coefficients in the $d_{\rm Ag} =$ 2-nm sample must be due to change in orientation between $\vec{M}_{\rm Fe}$ and $\overleftrightarrow{S}_{\rm CoO}$. Because the spin-current diffusion length in CoO (~6 nm [3]) is shorter than the 10 nm of CoO in our sample, the Py layer should not be relevant to spin-current absorption here. Although the FMR damping being greater when $\vec{M}_{\rm Fe} \parallel \overleftrightarrow{S}_{\rm CoO}$ than for $\vec{M}_{\rm Fe} \perp \overleftrightarrow{S}_{\rm CoO}$ is consistent with the spin-current anisotropy in AFM, one has to be careful when considering the FM/AFM coupling which could also result in an anisotropic FMR damping via other mechanisms [26–29].

To separate the Fe/CoO interlayer coupling effect from the spin-current anisotropy, we performed Fe FMR measurements on the $d_{\rm Ag} = 8$-nm sample where the 8-nm Ag is thick enough to diminish the Fe/CoO interlayer coupling but thin enough to permit spin-current transmission across the Ag. First, we find that the FMR field in the $d_{\rm Ag} = 8$-nm sample is identical for the cases of $\vec{M}_{\rm Fe} \parallel \overleftrightarrow{S}_{\rm CoO}$ and $\vec{M}_{\rm Fe} \perp \overleftrightarrow{S}_{\rm CoO}$ [Fig. 3(b)], confirming the vanished Fe/CoO interlayer coupling across 8-nm Ag, which agrees with the isotropy of the corresponding hysteresis loops in Figs. 2(a) and 2(b). Second, the FMR damping ($\alpha = 0.0057$) is greater than that from a Ag/Fe/Ag(001) reference film ($\alpha = 0.0034$) [Fig. 3(d)], showing that 8-nm Ag indeed is thin enough to permit spin-current transmission into the CoO layer. Finally, the identical damping ($\alpha = 0.0057$) within the accuracy of 0.0007 for the cases of $\vec{M}_{\rm Fe} \parallel \overleftrightarrow{S}_{\rm CoO}$ and $\vec{M}_{\rm Fe} \perp \overleftrightarrow{S}_{\rm CoO}$ [Fig. 3(d)] shows the absence of anisotropic FMR damping. By comparing the FMR results from the $d_{\rm Ag} =$ 2-nm and $d_{\rm Ag} = 8$-nm samples, the anisotropic damping of Fe FMR in the $d_{\rm Ag} = 2$ nm sample must come entirely from the Fe/CoO interlayer coupling effect rather than from any spin-current anisotropy. To further confirm this assertion, we measured the FMR damping coefficients systematically for the cases of $\vec{M}_{\rm Fe} \parallel \overleftrightarrow{S}_{\rm CoO}$ and $\vec{M}_{\rm Fe} \perp \overleftrightarrow{S}_{\rm CoO}$ as a function of Ag thickness. The result [Fig. 3(f)] shows that the damping coefficients for $\vec{M}_{\rm Fe} \parallel \overleftrightarrow{S}_{\rm CoO}$ and $\vec{M}_{\rm Fe} \perp \overleftrightarrow{S}_{\rm CoO}$ are different only for $d_{\rm Ag} < 4.5$ nm where there exists Fe/CoO interlayer coupling across the Ag spacer layer as evidenced by the enhanced $H_{\rm C}$ and $H_{\rm S}$ in the hysteresis loops [Fig. 3(e)]. Extracted from the FMR result, fourfold anisotropy of the Fe layer is about 496.2 Oe. The interlayer coupling-induced uniaxial anisotropy of Fe layer in $d_{\rm Ag} =$ 2-nm sample is about 549.1 Oe, which is consistent with the MOKE result [Fig. 2(b)].

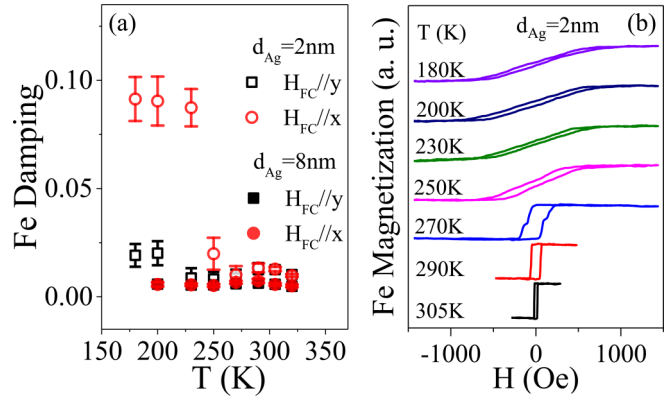

FIG. 4. (a) Fe FMR damping for $H_{\rm FC} \parallel x$ and $H_{\rm FC} \parallel y$ as a function of temperature from $d_{\rm Ag} = 2$- and $d_{\rm Ag} = 8$-nm samples. (b) Fe hysteresis loops of $d_{\rm Ag} = 2$ nm sample for $H \perp H_{\rm FC}$.

To further confirm that the anisotropic damping in samples with the Ag spacer layer below 4.5 nm is indeed from the Fe/CoO interlayer coupling, we performed a temperature-dependent study on the $d_{\rm Ag} = 2$-nm sample. Fe hysteresis loops [Fig. 4(b)] for $H \perp H_{\rm FC}$ show that the HA loop character (high saturation field and low remanence) evolves into an EA loop character (square-shape loop with a full remanence) above $T \sim 270$–290 K which corresponds to the CoO Néel temperature [46]. Correspondingly, the Fe FMR damping anisotropy between the two cases of $\vec{M}_{\rm Fe} \perp \overleftrightarrow{S}_{\rm CoO}$ and $\vec{M}_{\rm Fe} \parallel \overleftrightarrow{S}_{\rm CoO}$ is negligibly small above 270 K and develops rapidly below 270 K in the $d_{\rm Ag} = 2$-nm sample. In contrast, the Fe FMR damping exhibits negligible anisotropy across the entire temperature range for the $d_{\rm Ag} = 8$-nm sample. We also note that the Fe FMR damping coefficients in both $d_{\rm Ag} = 2$- and $d_{\rm Ag} = 8$-nm samples seem to show a broad peak in the temperature range of ~270–300 K. Because these damping values are approaching the limits of accuracy for the FMR measurements, we hesitate to claim this peak as significant. However, it is worth mentioning that an enhancement of

spin-current injection into AFM CoO in the vicinity of CoO Néel temperature has been reported in the literature and has been attributed to excitation of thermal magnons in CoO [3,4,19]. Based on the damping anisotropy between $\vec{M}_{\mathrm{Fe}} \perp \overleftrightarrow{S}_{\mathrm{CoO}}$ and $\vec{M}_{\mathrm{Fe}} \parallel \overleftrightarrow{S}_{\mathrm{CoO}}$ in the $d_{\mathrm{Ag}} = 2$-nm sample at low temperature, which is much greater than the damping in the $d_{\mathrm{Ag}} = 8$-nm sample, we further conclude that this anisotropic damping is entirely from interlayer coupling rather than any spin-current anisotropy. Despite the weak FMR signal, our result is enough to support our main conclusion here. Finally we note that there have been reports on anisotropic damping in FM/AFM systems via other interfacial mechanisms, such as two-magnon scattering [28,29]. The current work is focused on separating the effects of spin-current anisotropy from those of interlayer coupling in terms of their influence on magnetic damping anisotropy, reserving a more detailed study of the exact nature of interfacial coupling to future studies.

IV. CONCLUSIONS

In summary, we studied the damping of Fe ferromagnetic resonance in Py/CoO/Ag/Fe multilayer samples. By determining the CoO Néel vector orientation using XMLD spectroscopy and separating the interlayer coupling effect from the spin-current effect, we show that there is no detectable spin-current anisotropy within the accuracy of 0.0007 of the damping values for CoO spins parallel and perpendicular to the Fe magnetization. All observed anisotropic Fe FMR damping is entirely due to the Fe/CoO interlayer coupling across the Ag spacer layer. Our result on the absence of spin-current anisotropy relative to the CoO Néel vector orientation establishes a criterion for future studies on the spin current in antiferromagnetic insulators.

ACKNOWLEDGMENTS

The project was primarily supported by US Department of Energy (DOE), Office of Science, Office of Basic Energy Sciences, Materials Sciences and Engineering Division under Contract No. DE-AC02-05CH112311 (van der Waals heterostructures program, KCWF16). This work was also supported by King Abdullah University of Science and Technology (KAUST), Office of Sponsored Research (OSR) and under the Award No. OSR-2017-CRG6-3427, Future Materials Discovery Program through the National Research Foundation of Korea (Grant No. 2015M3D1A1070467), Science Research Center Program through the National Research Foundation of Korea (Grant No. 2015R1A5A1009962). This research used resources of the Advanced Light Source, which is a DOE Office of Science User Facility under Contract No. DE-AC02-05CH11231.

[1] H. Wang, C. Du, P. C. Hammel, and F. Yang, Phys. Rev. Lett. **113**, 097202 (2014).
[2] C. Hahn, G. de Loubens, V. V. Naletov, J. Ben Youssef, O. Klein, and M. Viret, Europhys. Lett. **108**, 57005 (2014).
[3] W. Lin, K. Chen, S. Zhang, and C. L. Chien, Phys. Rev. Lett. **116**, 186601 (2016).
[4] Z. Qiu, J. Li, D. Hou, E. Arenholz, A. T. N'Diaye, A. Tan, K. Uchida, K. Sato, S. Okamoto, Y. Tserkovnyak, Z. Q. Qiu, and E. Saitoh, Nat. Commun. **7**, 12670 (2016).
[5] K. M. D. Hals, Y. Tserkovnyak, and A. Brataas, Phys. Rev. Lett. **106**, 107206 (2011).
[6] M. W Daniels, W. Guo, G. M. Stocks, D. Xiao, and J. Xiao, New J. Phys. **17**, 103039 (2015).
[7] S. M. Rezende, R. L. Rodríguez-Suárez, and A. Azevedo, Phys. Rev. B **93**, 054412 (2016).
[8] K. Chen, W. Lin, C. L. Chien, and S. Zhang, Phys. Rev. B **94**, 054413 (2016).
[9] S. Takei, T. Moriyama, T. Ono, and Y. Tserkovnyak, Phys. Rev. B **92**, 020409(R) (2015).
[10] T. Kampfrath, A. Sell, G. Klatt, A. Pashkin, S. Mährlein, T. Dekorsy, M. Wolf, M. Fiebig, A. Leitenstorfer, and R. Huber, Nat. Photon. **5**, 31 (2011).
[11] R. Cheng, J. Xiao, Q. Niu, and A. Brataas, Phys. Rev. Lett. **113**, 057601 (2014).
[12] T. Moriyama, M. Kamiya, K. Oda, K. Tanaka, K.-J. Kim, and T. Ono, Phys. Rev. Lett. **119**, 267204 (2017).
[13] A. A. Baker, A. I. Figueroa, C. J. Love, S. A. Cavill, T. Hesjedal, and G. van der Laan, Phys. Rev. Lett. **116**, 047201 (2016).
[14] R. Lebrun, A. Ross, S. A. Bender, A. Qaiumzadeh, L. Baldrati, J. Cramer, A. Brataas, R. A. Duine, and M. Kläui, Nature (London) **561**, 222 (2018).
[15] Z. Qiu, D. Hou, J. Barker, K. Yamamoto, O. Gomonay, and E. Saitoh, Nat. Mater. **17**, 577 (2018).
[16] D. M. Polishchuk, A. Kamra, T. I. Polek, A. Brataas, and V. Korenivski, Phys. Rev. Lett. **123**, 247201 (2019).
[17] D. Hou, Z. Qiu, J. Barker, K. Sato, K. Yamamoto, S. Vélez, J. M. Gomez-Perez, L. E. Hueso, F. Casanova, and E. Saitoh, Phys. Rev. Lett. **118**, 147202 (2017).
[18] H. Saglam, J. C. Rojas-Sanchez, S. Petit, M. Hehn, W. Zhang, J. E. Pearson, S. Mangin, and A. Hoffmann, Phys. Rev. B **98**, 094407 (2018).
[19] Q. Li, M. Yang, C. Klewe, P. Shafer, A. T. N'Diaye, D. Hou, T. Y. Wang, N. Gao, E. Saitoh, C. Hwang, R. J. Hicken, J. Li, E. Arenholz, and Z. Q. Qiu, Nat. Commun. **10**, 5265 (2019).
[20] B. Khodadadi, Y. Lim, D. A. Smith, R. W. Greening, Y. Zheng, Z. Diao, C. Kaiser, and S. Emori, Phys. Rev. B **99**, 024435 (2019).
[21] E. Arenholz, G. van der Laan, R. V. Chopdekar, and Y. Suzuki, Phys. Rev. Lett. **98**, 197201 (2007).
[22] J. Wu, J. S. Park, W. Kim, E. Arenholz, M. Liberati, A. Scholl, Y. Z. Wu, C. Hwang, and Z. Q. Qiu, Phys. Rev. Lett. **104**, 217204 (2010).
[23] Y. Takamura, E. Folven, J. B. R. Shu, K. R. Lukes, B. Li, A. Scholl, A. T. Young, S. T. Retterer, T. Tybell, and J. K. Grepstad, Phys. Rev. Lett. **111**, 107201 (2013).

[24] Y. M. Lu, Y. Choi, C. M. Ortega, X. M. Cheng, J. W. Cai, S. Y. Huang, L. Sun, and C. L. Chien, Phys. Rev. Lett. **110**, 147207 (2013).
[25] T. K. H. Pham, M. Ribeiro, J. H. Park, N. J. Lee, K. H. Kang, E. Park, V. Q. Nguyen, A. Michel, C. S. Yoon, S. Cho, and T. H. Kim, Sci. Rep. **8**, 13907 (2018).
[26] R. D. McMichael, M. D. Stiles, P. J. Chen, and W. F. Egelhoff, J. Appl. Phys. **83**, 7037 (1998).
[27] M. J. Pechan, D. Bennett, N. Teng, C. Leighton, J. Nogués, and I. K. Schuller, Phys. Rev. B **65**, 064410 (2002).
[28] T. Mewes, R. L. Stamps, H. Lee, E. Edwards, M. Bradford, C. K. A. Mewes, Z. Tadisina, and S. Gupta, IEEE Magn. Lett. **1**, 3500204 (2010).
[29] J. Beik Mohammadi, J. M. Jones, S. Paul, B. Khodadadi, C. K. A. Mewes, T. Mewes, and C. Kaiser, Phys. Rev. B **95**, 064414 (2017).
[30] L. Chen, S. Mankovsky, S. Wimmer, M. A. W. Schoen, H. S. Körner, M. Kronseder, D. Schuh, D. Bougeard, H. Ebert, D. Weiss, and C. H. Back, Nat. Phys. **14**, 490 (2018).
[31] Y. Li, F. Zeng, S. S.-L. Zhang, H. Shin, H. Saglam, V. Karakas, O. Ozatay, J. E. Pearson, O. G. Heinonen, Y. Wu, A. Hoffmann, and W. Zhang, Phys. Rev. Lett. **122**, 117203 (2019).
[32] R. Urban, G. Woltersdorf, and B. Heinrich, Phys. Rev. Lett. **87**, 217204 (2001).
[33] B. Heinrich, Y. Tserkovnyak, G. Woltersdorf, A. Brataas, R. Urban, and G. E.W. Bauer, Phys. Rev. Lett. **90**, 187601 (2003).
[34] P. Merodio, A. Ghosh, C. Lemonias, E. Gautier, U. Ebels, M. Chshiev, H. Béa, V. Baltz, and W. E. Bailey, Appl. Phys. Lett. **104**, 032406 (2014).
[35] W. Zhang, M. B. Jungfleisch, W. Jiang, J. E. Pearson, A. Hoffmann, F. Freimuth, and Y. Mokrousov, Phys. Rev. Lett. **113**, 196602 (2014).
[36] L. Frangou, S. Oyarzún, S. Auffret, L. Vila, S. Gambarelli, and V. Baltz, Phys. Rev. Lett. **116**, 077203 (2016).
[37] W. N. Cao, J. Li, G. Chen, J. Zhu, C. R. Hu, and Y. Z. Wu, Appl. Phys. Lett. **98**, 262506 (2011).
[38] B. Kardasz, O. Mosendz, B. Heinrich, Z. Liu, and M. Freeman, J. Appl. Phys. **103**, 07C509 (2008).
[39] R. E. Camley, Z. Celinski, and R. L. Stamps, in *Magnetism of Surfaces, Interfaces, and Nanoscale Materials* (Elsevier, Amsterdam, 2015), Vol. 5, Chap. 10, p. 428.
[40] M. H. Seavey and P. E. Tannenwald, J. Appl. Phys. **29**, 292 (1958).
[41] Q. Li, G. Chen, T. P. Ma, J. Zhu, A. T. N'Diaye, L. Sun, T. Gu, Y. Huo, J. H. Liang, R. W. Li, C. Won, H. F. Ding, Z. Q. Qiu, and Y. Z. Wu, Phys. Rev. B **91**, 134428 (2015).
[42] W. Weber, A. Bischof, R. Allenspach, Ch. Würsch, C. H. Back, and D. Pescia, Phys. Rev. Lett. **76**, 3424 (1996).
[43] Y. Meng, J. Li, P.-A. Glans, C. A. Jenkins, E. Arenholz, A. Tan, J. Gibbons, J. S. Park, C. Hwang, H. W. Zhao, and Z. Q. Qiu, Phys. Rev. B **85**, 014425 (2012).
[44] G. van der Laan, E. Arenholz, R. V. Chopdekar, and Y. Suzuki, Phys. Rev. B **77**, 064407 (2008).
[45] B. Heinrich, J. F. Cochran, and R. Hasegawa, J. Appl. Phys. **57**, 3690 (1985).
[46] Q. Li, T. Gu, J. Zhu, Z. Ding, J. X. Li, J. H. Liang, Y. M. Luo, Z. Hu, C. Y. Hua, H.-J. Lin, T. W. Pi, C. Won, and Y. Z. Wu, Phys. Rev. B **91**, 104424 (2015).